Mikko Tuohimaa

Development and Performance Analysis of a Novel Pulse Oximetry Measurement Circuit

School of Electrical Engineering

Thesis submitted for examination for the degree of Master of Science in Technology.

Espoo 30.3.2012

Thesis supervisor:

Prof. Arto Visala

Thesis instructor:

M.Sc. (Tech.) Sakari Lamminmäki

Aalto University
School of Electrical Engineering

AALTO UNIVERSITY
SCHOOL OF ELECTRICAL ENGINEERING

ABSTRACT OF THE
MASTER'S THESIS

Author: Mikko Tuohimaa

Title: Development and Performance Analysis of a Novel Pulse Oximetry Measurement Circuit

Date: 30.3.2012 Language: English Number of pages:7+57

Department of Automation and Systems Technology

Professorship: Autonomous Systems Code: AS-84

Supervisor: Prof. Arto Visala

Instructor: M.Sc. (Tech.) Sakari Lamminmäki

All life, including human tissues, depends on sufficient oxygenation. Severe, irreversible cell damage can occur if oxygen supply is prohibited due to the fact that the tissues have only minimal oxygen reserves. Therefore it's essential to monitor oxygen delivery during anesthesia, critical care and other high-risk situations.
Pulse oximetry is a non-invasive optical method used for continuous measurement of oxygen saturation of arterial blood. Infrared and red monochromatic light are transmitted through tissue and the transmittance measured with a photodetector – due to the fact that hemoglobin's absorption spectrum depends on if it's carrying oxygen or not, the ratio of transmittances can be used to determine the percentage of hemoglobin that is oxygenated. Additionally, the measurement can be focused on arterial blood by examining the pulsatile waveform induced by cardiac activity. The result is a good indicator of oxygen deprivation and it's been used in clinical care for decades, the devices usually having been large and static multi-parameter monitors. GE Healthcare is developing new pulse oximetry solutions for a range of applications with different power and performance requirements.
The goal of this thesis was to verify that a new small pulse oximetry measurement solution reaches the strict design specifications set for it, including a very low noise level, a high dynamic range and the ability to function in an extremely low power mode. The means to this goal was to develop the software used by this novel front-end, assess the performance of the system as a whole and use regression analysis to identify possible noise sources and other defects in the signal chain. Additionally, based on the measurements, a relationship connecting various operating limits and minimum power consumption was formed. The outputs of the thesis are the new evaluation process using a black-box approach, two bugs found in the receiver signal chain thanks to the aforementioned process and the notion that the new front-end can be accepted if the issues identified are fixed.

Keywords: Pulse Oximetry, S_pO_2 , Optical Measurement, Measurement Circuit, Microcontroller, Regression Analysis, Black Box, System Testing

Preface

This thesis is the culmination point of seven years of studying in Helsinki University of Technology, later known as Aalto University. It has been quite a ride.

The old saying is that the university educates you in science but the student community educates you in life. I've found this most accurate during my stay in Otaniemi campus and I'd like to thank everyone with whom I've had the pleasure to study, party, talk politics, talk nonsense, laugh, cry, love, hate, et cetera and so forth. Without all that I probably would've graduated a long time ago but without the best memories of my life.

Most of those memories and fine moments have something to do with one of three instances: the Guild of Automation and Systems Technology (especially the board of 2007), the 2007 Committee of Freshman Education and Luolamiehet. You all know what I'm talking about. Also thanks to the AS freshmen of 2005, especially Tuomas and Kalle, for taking the dive with me into the university realm.

GE Healthcare deserves special thanks; I feel privileged to have been able to work on a very interesting subject with a lot of responsibility, doing stuff that matters. Also the employees of the Circulatory team are not only very bright people but also great fun to work with. Extra special thanks go to Sakari Lamminmäki for having great confidence in me and my abilities which showed in letting me work very independently and follow my intuition.

Finally, thanks, mom and dad, for showing nothing but support in the decisions I've made throughout the years.

Espoo 30.3.2012

Mikko T. A. Tuohimaa

Contents

Symbols and abbreviations

Symbols

f	Frequency
I, I_0, I_λ	Light intensity, incident light intensity, light intensity at wavelength λ
m	I_{AC}/I_{DC}; signal modulation coefficient
p	Partial pressure
p_{O_2}	Partial pressure of oxygen
p_{CO_2}	Partial pressure of carbon dioxide
R	m_R/m_{IR}; the ratio of the modulations of the red and the IR signals
α	The portion of plethysmographic waveform energy that is focused on its fundamental frequency
β	The portion of noise energy that is focused on the pleth fundamental frequency
ϵ	Extinction coefficient
σ	Standard deviation
τ	Time period, interval

Operators

$\frac{\mathrm{d}}{\mathrm{d}t}$	The derivative in respect to the variable t
$\frac{\partial}{\partial t}$	The partial derivative in respect to the variable t
$\sum_i$	Sum over the index i

Abbreviations

A/D, ADC	Analog to Digital, Analog to Digital Converter
BW	Bandwidth, frequency range
CO	Carbon monoxide
CO_2	Carbon dioxide
COHb	Carboxyhemoglobin
D/A, DAC	Digital to Analog, Digital to Analog Converter
DMA	Direct Memory Access
EEPROM	Electronically Erasable Programmable Read-Only Memory
GE	General Electric
GEHC	GE Healthcare
GPIO	General Purpose Input/Output
Hb	Hemoglobin
ICU	Intensive Care Unit
I/O	Input/Output
LED	Light Emitting Diode
LSB	Least Significant Bit/Byte
MetHb	Methemoglobin
MSB	Most Significant Bit/Byte
O_2	Oxygen
O_2Hb	Oxygenated hemoglobin (oxyhemoglobin)
OR	Operating Room
RAM	Random Access Memory
RBC	Red Blood Cell
RHb	Reduced (deoxygenated) hemoglobin
RISC	Reduced Instruction Set Computer
RMS	Root-Mean-Square
RoHS	Reduction of Hazardous Substances
S_aO_2	Arterial blood oxygen saturation
SNR	Signal to Noise Ratio
SPI	Serial Peripheral Interface Bus
S_pO_2	Arterial blood hemoglobin oxygen saturation measured with a pulse oximeter
UART	Universal Asynchronous Receiver/Transmitter
USCI	Universal Serial Communication Interface

1 Introduction

All life, including human tissues, depends on sufficient oxygenation. Severe, irreversible cell damage can occur if oxygen supply is prohibited due to the fact that the tissues have only minimal oxygen reserves. Therefore it's essential to monitor oxygen delivery during anesthesia, critical care and other high-risk situations.

Pulse oximetry is a non-invasive optical method used for continuous measurement of oxygen saturation of arterial blood. It's a good indicator of oxygen deprivation and it has been used in clinical care for decades, the devices usually having been large and static multi-parameter monitors. GE Healthcare is developing new pulse oximetry solutions for a range of applications with different power and performance requirements.

The core of the measurement is the measurement circuit, also known as the front-end. It acts on the device-patient interface producing as high-quality measurements as possible. The signal processing algorithm relies on the incoming signal being accurate and noise-free, and therefore the performance of the front-end will directly translate into more accurate algorithm output.

The goal of this thesis is to verify that a new small pulse oximetry measurement solution reaches the strict design specifications set for it, including a very low noise level, a high dynamic range and the ability to function in an extremely low power mode. The means to this goal is to develop the software used by this novel front-end, assess the performance of the system as a whole and use regression analysis to identify possible noise sources and other defects in the signal chain. Additionally, based on the measurements, a relationship connecting various operating limits and minimum power consumption is formed. The output of the thesis is if the new front-end can be accepted or not and the rationale behind the decision, and if the front-end is deemed unsatisfactory, an analysis on which components are decreasing the system's performance.

The front-end evaluation is done using a black-box approach. This is necessary since the front-end hardware is so tightly packed and shielded that it's not practically possible to measure anything in the middle of the signal chain – therefore the only data source used is the system's own output. This is a new approach in assessing subsystem-specific performance; the process developed will be useful in the future as miniaturization becomes more and more common in the industry.

In the first part of the thesis an introduction to the physiological basis of tissue oxygenation is given and the principles of pulse oximetry are explained. Further on, a theoretical noise performance specification is derived for the new circuit and the main components contributing to total system noise are listed. The new measurement circuit is introduced in chapter 5, the process for its evaluation drafted in chapter 6 and the results and their interpretation shown in chapter 7.

2 Tissue Oxygenation

The metabolic reactions that fuel living cells need a continuous supply of oxygen (O_2). These reactions oxidize nutrient molecules for energy and as a byproduct produce carbon dioxide (CO_2) which has to be removed to prevent toxic acidity in cells. The exchange of these gases, O_2 and CO_2, relies on the cooperation of the cardiovascular and respiratory systems, either of which failing would result in severe consequences: severe, irreversible cell damage can occur if oxygen supply is prohibited due to the fact that the tissues have only minimal oxygen reserves – for example the brain will suffer from continued oxygen deprivation in a matter of minutes. Therefore it's essential to monitor oxygen delivery during anesthesia, critical care and other high-risk situations. [1]

2.1 The Cardiovascular System

The primary function of the cardiovascular system is to deliver oxygen, nutrients, signal molecules and other substances to all tissues and cells throughout the body and to remove the waste produced by them, such as carbon dioxide (CO_2). In short, the cardiovascular system is a network of blood vessels that provides a means of transportation for these substances between the tissues and functional organs, powered by the heart. [1]

2.1.1 Structure and Operation of the Cardiovascular System

The mammal cardiovascular system is composed of two circuits, the pulmonary and the systemic one, and the heart that simultaneously pumps blood into them both (see figure 1). The pulmonary loop goes from the right ventricle of the heart to the lungs where blood is oxygenated, carbon dioxide is extracted and the blood directed back to the left atrium. Fresh, oxygen rich blood is then pumped by the left ventricle into systemic circulation through arteries and finally into capillaries where the exchange of blood-carried substances takes place. The now deoxygenated blood is carried back to the heart by veins and the loop continues.

The cardiovascular system also includes a blood flow regulation system that utilizes several interconnected negative feedback systems that work both together and in parallel to adjust the amount and the distribution of blood flow within the body. The main function of this system is to ensure that all tissues receive adequate oxygenation while optimizing overall thermoregulation and energy consumption.

The control center for the cardiovascular system is the cardiovascular center in the brain stem. It receives input signals from various sensory receptors all over the system monitoring blood pressure, blood volume, blood acidity (pH), body temperature and body movements. Based on this input, the cardiovascular center adjusts the cardiac output (heart rate and stroke volume) and the resistance (diameter) of blood vessels to maintain an adequate blood pressure and tissue oxygenation in all parts of the system. Cardiac output, being defined as the product of heart rate and stroke volume, is essentially the total flow of blood through the heart and thus is

Figure 1: *The structure of the cardiovascular system. [2]*

associated with the total oxygen demand of the body. Blood vessel resistance, on the other hand, is a localized quantity and the resistance distribution between organs or body parts rarely is even. The resistance is controlled by the cardiovascular center in the brain using smooth muscles lining the walls of blood vessels either to constrict or to dilate them. [1]

2.1.2 Blood and Hemoglobin

Blood has two primary components. The liquid part with different proteins and other substances dissolved in it is called *plasma*, and it usually constitutes about 55% of total blood volume. The other 45% are blood cells and cell fragments out of which normally over 99% are red blood cells (*RBCs*). The rest are white blood cells and platelets. Therefore the percentage of total blood volume occupied by RBCs is normally in the range of 38-54% and is called the *hematocrit*. [1]

Oxygen, in its basic molecular form, doesn't dissolve easily in plasma. That is the reason red blood cells, also known as *erythrocytes* and seen in figure 2, have the sole purpose of oxygen transportation and are highly specialized for it. Their bi-concave shape and the lack of most intracellular organs give them excellent surface-to-volume ratio for gas exchange by diffusion and frees the intracellular space for hemoglobin. Due to this, each microscopical erythrocyte is able to contain about 280 million

Figure 2: *Hemoglobin molecule and the red blood cell. [3, 4]*

hemoglobin molecules - roughly a third of the cell's mass. [1]

A hemoglobin molecule is a protein complex with four polypeptide chains and four non-protein pigments called *hemes*. Each heme is associated with a polypeptide chain and contains a Fe^{2+} ion, able to reversibly bind an oxygen molecule; oxygen is picked up in the lungs and the reaction is reversed in the tissues, releasing the oxygen molecule that diffuses first into the interstitial fluid and then into cells. The polypeptide chains of hemoglobin also take care of transferring about 23% of the carbon dioxide produced in cells, the rest being dissolved into plasma. [1]

2.1.3 Dysfunctional Hemoglobins

The vast majority of hemoglobin in circulation is either fully oxygenated hemoglobin (*oxyhemoglobin*, O_2Hb) or reduced hemoglobin that isn't oxygen-saturated (also called *deoxyhemoglobin*). These two hemoglobin species are referred to as *functional hemoglobins* because they can execute the oxygen transportation task. In addition to these, there exist several other species of hemoglobin in the blood that have lost their oxygen carrying capability and are thus called *dysfunctional hemoglobins* (*dyshemoglobins*). Normally dyshemoglobins constitute less than 3% of total hemoglobin content, a level that doesn't really affect oxygenation. There are some conditions, though, where the concentration of dyshemoglobins may rise significantly, reducing the amount of functional hemoglobin available and so endangering tissue oxygenation.

Dyshemoglobins are modified hemoglobins that form when functional hemoglobin reacts with other substances, including carbon monoxide and hydrogen sulfide. The most common dyshemoglobin, carboxyhemoglobin (COHb), is formed when the process that normally binds oxygen to hemoglobin captures a carbon monoxide molecule instead. Carbon monoxide's binding affinity in this process is ca. 210-fold compared to oxygen's, rendering the hemoglobin molecule essentially inert for oxygen. Another common dyshemoglobin is methemoglobin (MetHb) that is the result of an oxidation reaction of the hemoglobin molecule: when the iron ion of the heme is oxidized from Fe^{2+} to Fe^{3+}, the heme loses its ability to bind oxygen and is rendered useless for its oxygenation purpose. [5]

2.2 The Respiratory System

In biology, respiration is defined as the sum of chemical and physical processes in an organism by which oxygen is conveyed to tissues and the oxidation products are given off to the parent medium (in the case of mammals, air). It can be divided into three elementary steps, which are pulmonary ventilation, external respiration and internal respiration. *The respiratory system* is responsible for the first two (air-blood interface), the main objective being the gas exchange between air and blood. The latter one, internal respiration, refers to the exchange of gases in systemic capillaries, being mostly a responsibility of the cardiovascular system. [1]

2.2.1 Anatomy of the Respiratory System

The respiratory system consists of the nose, pharynx (throat), larynx (voice box), trachea (windpipe), bronchi and lungs (figure 3). Its main function is to get fresh air into contact with as much diffusion surface as possible which is achieved by the *conducting portion* of the respiratory system directing air to lungs, which in turn have a huge number of extremely small air conduits that maximize the air's surface-to-volume ratio. This is essential for effective gas exchange through the respiratory membrane since the amount of diffused gases is directly proportional to the diffusion surface, not total volume. It's figurative that the average total lung volume in an adult is between 5 and 6 liters while the total surface area is roughly 70 m^2. This is the equivalent of a standard bucket and a tennis court. [1]

Pulmonary ventilation, commonly known as breathing, is driven by the contrac-

Figure 3: *The human respiratory system. [6]*

tion and relaxation of respiratory muscles. The muscles, mainly the diaphragm, increase the volume of the thoracic cavity when contracting, causing a pressure difference between the lungs and the atmosphere which forces air to flow into the lungs. When said muscles relax the thoracic cavity returns to its normal volume and air is forced out.

The diaphragm and other respiratory muscles are skeletal muscles, which means they must be controlled directly with nerve impulses. Most of the time this control is involuntary but can be overridden by voluntary actions. The respiratory center is located in the brain stem and is functionally divided into three areas: the *medullary rhythmicity area* provides the basic rhythm of respiration but it can be modified, along with the volume of inspiration, by the *pneumotaxic* and *apneustic areas* according to inputs from other parts of the brain and sensory receptors. Like blood circulation, also respiration is regulated in response to various signals originating from all around the body and measuring quantities such as oxygen and carbon dioxide levels and blood pressure. In fact, some of these receptors are multifunctional, being used by both the respiratory and the cardiovascular centers. [1]

2.2.2 Gas Exchange

The transfer of oxygen and carbon dioxide in the air-blood and the blood-tissue interfaces is based on the differences in partial pressures of these gases throughout the cardiovascular and respiratory systems. Therefore the physics of partial pressures is worth looking into.

In gas mixtures, such as air, each component gas has a partial pressure that is independent of the other gases and is denoted as p - it's the pressure the gas would have if it alone occupied the volume. Therefore the sum of all the partial pressures equals the total pressure of the gas mixture. Diffusion can be modelled easily with partial pressures: when there's a partial pressure gradient for a gas, there will be a net flow of that gas in the direction of the gradient until equilibrium is reached.

The exchange of gases in alveoli, as well as in systemic capillaries, is driven by diffusion. Since the partial pressure of oxygen (p_{O_2}) is higher in the air in alveoli (ca. 140 hPa at sea level) than in the blood entering the pulmonary capillaries (ca. 50 hPa) [7], oxygen diffuses through the respiratory membrane into the blood. The p_{O_2} in the interstitial fluid in tissues is even lower than in the blood, causing oxygen molecules to diffuse through the capillary wall. Carbon dioxide behaves similarly but in the opposite direction due to its higher concentration in tissues compared to air.

In addition to diffusion, partial pressure is also the most important factor in determining how oxygen combines with hemoglobin and therefore tremendously affects the efficiency of oxygen transportation. This is due to the fact that over 98% of transported oxygen is bound to hemoglobin since oxygen doesn't dissolve easily in water. The binding affinity is dependent on the p_{O_2} of blood according to the oxygen-hemoglobin dissociation curve in figure 4, which shows the oxygen saturation (percentage of oxyhemoglobin out of total functional hemoglobin) as a function of p_{O_2}. In the alveolar p_{O_2}, 140 hPa (105 mmHg), oxygen binds very well with

hemoglobin, resulting in a saturation level of 97% of arterial blood. When the blood reaches the systemic capillaries the diffusion starts, lowering the blood's p_{O_2} and inducing oxygen dissociation from hemoglobin. After the gas exchange the p_{O_2} of venous blood is about 50 hPa (40 mmHg, equal to the level in tissues), meaning that hemoglobin is still roughly 75% saturated. In conclusion, only 25% of the blood's total oxygen content is released in tissues. [1]

Figure 4: *Oxygen dissociation curve of hemoglobin. [8]*

2.3 Hypoxia

Hypoxia, by definition, is a condition where tissue lacks adequate oxygen supply. It can be a local or a general condition depending on the circumstances. In all cases, though, disturbing the oxygen delivery to cells greatly disrupts cell metabolism, eventually leading to cell necrosis and tissue damage. This may occur in just a few minutes, first affecting major oxygen consumers such as the brain, the heart and other vital organs. It often happens that the first symptoms of hypoxia, mainly skin discoloration in the case of unconscious patients, go unnoticed because as subtle changes they are difficult to recognize and measure; when the condition is finally diagnosed after worsened symptoms it may already be too late.

The are various possible underlying reasons for hypoxia, related to different parts of the oxygen delivery system. They include, but are not limited to, for example low p_{O_2} in arterial blood due to low p_{O_2} in air in high altitudes or closed spaces (hypoxic hypoxia), low amount of functional hemoglobin in blood due to poisoning or

anemic conditions (anemic hypoxia), poor or blocked blood flow to tissues (stagnant hypoxia) or tissues being unable to utilize oxygen (histotoxic hypoxia). The reason for hypoxia could even be as simple as the patient not breathing. [1, 5]

2.4 Anesthesia

When a patient is kept in anesthesia e.g. for a surgical procedure it's common that the patient has been intubated, having a respirator taking care of the patient's breathing. In these conditions it is extremely important to monitor the patient's S_pO_2 since otherwise the machine can't compensate for increased or decreased oxygen consumption as a healthy person would by breathing harder. Also leaks and other malfunctions that severely affect the patient's respiratory function can happen. [9]

Another factor is the importance of pulse oximetry in the recovery room. It often happens that a patient recovering from anesthesia has received a slight overdose of the anesthetic agent or for other reasons exhibits reduced respiratory function. Detecting such conditions greatly improves patient outcome, saving them from unnecessary complications, and therefore pulse oximetry monitoring is recommended as a standard procedure also for recovery. [10]

3 Pulse Oximetry

Pulse oximetry is a non-invasive optical method used for continuous measurement of oxygen saturation of arterial blood. It has become a monitoring standard for patients in critical care and anesthesia during the past two decades because of its capability to measure the oxygen saturation of arterial blood continuously and non-invasively, providing vital information about the cardiorespiratory function of the patient and thus making it a convenient, safe and effective source of alarms. In many applications it is the fastest and the most efficient way to detect hypoxia and other life-threatening conditions that require a fast response. [5]

The method is rather accurate: when the arterial oxygenation is over 70%, pulse oximeters usually provide a measurement that differentiates from the actual oxygenation by less than 3%-units. This level of accuracy is enough for most applications as the usual operating range is well over 80% level. [11]

The history of oximetry dates back roughly 70 years. The first motive for its development was to monitor fighter pilots when flying at high altitudes during World War II - at high speeds and g-forces their very life depended on them staying conscious. The early devices used mercury lamps, different filters and a spectrophotometer and were not that accurate over time, but they served their purpose even though they were unable to differentiate between arterial and venous blood. [12]

The era of modern pulse oximetry saw light in the early 1970's when it was discovered that the pulsatile nature of the oximeter output could be used to extract arterial oxygen saturation from the signal. Soon after that, an American corporation called Biox made another breakthrough by introducing LEDs as the light source in oximeters; incidentally, Biox is now a part of GE through several acquisitions. The technology has evolved tremendously since the early days but the principle has remained the same since the 1980's. In addition to reducing size and cost, the method has been extended by adding wavelengths to measure total hemoglobin concentration and other blood parameters as well as improving the accuracy of basic S_pO_2, but the standard two-wavelength solution for measuring the percentage of arterial oxyhemoglobin is still by far the most commonly used one. [13]

3.1 Theory of Pulse Oximetry

An oximeter is physically little more than a light absorption meter. Placed on two sides of a tissue bed, it emits monochromatic light from one side and measures the light intensity on the other side. The operation is repeated with another wavelength. The absorption rates of the two wavelengths are different due to the uneven absorption spectra of different types of hemoglobin (figure 5) and the ratio of the absorptions can be used directly to estimate blood hemoglobin oxygenation. Unfortunately the resulting figure represents the sum of arterial and venous blood and the tissue bed itself and without carefully calibrating the device for each patient doesn't tell the observer much about the patient's condition. A signal processing method must be used to extract the arterial blood hemoglobin oxygenation from the total value.

The wavelength range over which this method can be used is limited between 600 and 1300 nm. At wavelengths shorter than 600 nm a large portion of the light is absorbed into the melanin of the skin, whereas wavelengths over 1300 nm are absorbed by water in tissues. The most commonly used wavelengths in two-wavelength systems are 660 nm and 940 nm - they are roughly the local absorption minimum and maximum, respectively, of oxyhemoglobin, and on the other hand deoxyhemoglobin's absorption spectrum is a descending one on that range (figure 5). Therefore these two wavelengths offer the best resolution available for differentiating between oxyhemoglobin and deoxyhemoglobin.

Figure 5: *The absorbance spectra of different species of hemoglobins. [14]*

The basis of pulse oximetry lies on photoplethysmography which is an optical method of measuring the volume change of a microvascular bed of tissue. A plethysmographic signal, shown in figure 6, is usually obtained by transmitting light through an extremity such as a fingertip or an earlobe and measuring the throughput on the other side as explained before. The signal waveform is generated by the cyclic changes in the absorbance of the tissue, being mostly due to pulsatile arterial blood volume induced by cardiac activity. This waveform is often known as the AC component of the plethysmographic signal and its amplitude is usually between 1-10% of the total signal, illustrated in figure 7. The rest of the light is absorbed by or reflected by different tissues and non-pulsating venous blood, causing a large *quasi-DC* offset in the signal. This offset is usually plainly referred to as the DC component since even though factors such as respiratory activity, sympathetic nervous system activity and thermoregulation can induce some variance in it, the

changes are much slower than the one induced by the heart. [15]

Figure 6: *A photoplethysmographic signal shown with a simultaneous ECG signal. [16]*

The measurement principle of photoplethysmography is founded on the Beer-Lambert law that describes light attenuation through a sample of homogeneous non-scattering medium hosting an absorbent:

$$I = I_0 e^{-\epsilon_\lambda \cdot c \cdot l}, \tag{1}$$

where I is the intensity of transmitted light, I_0 is the initial light intensity, ϵ_λ the extinction coefficient of the absorbent at the wavelength λ, c the concentration of the absorbent and l the optical path length of light (in other words, the thickness of the medium). If more than one absorbent is present in the medium, the total light attenuation can be obtained as a linear superposition of attenuations of each absorbent. Transmittance is defined as the ratio of transmitted and the initial light intensity, and absorbance as the negative natural logarithm of transmittance, which can be expressed as:

$$T = \frac{I}{I_0} = e^{-\epsilon_\lambda \cdot c \cdot l} \tag{2}$$

$$A = -lnT = \epsilon_\lambda \cdot c \cdot l \tag{3}$$

Since in pulse oximetry we're only interested in the time variant part of the absorbance that relates to the pulsatile arterial blood, the time-dependent AC component of the absorbance can be separated from this model by differentiating equation (3). In the case of monochromatic light, $I = I_\lambda$, the equation takes the following form:

Figure 7: *A demonstrative illustration of absorbance components in photoplethysmographic measurement (not in scale): the AC amplitude of the signal is small compared to the DC level, usually in the range of 1-10%.*

$$\frac{\partial A_\lambda}{\partial t} = -\frac{\partial I_\lambda}{\partial t \cdot I_\lambda} = \epsilon_\lambda \cdot c \cdot \frac{\partial l}{\partial t}. \tag{4}$$

The total differential absorbance for a given wavelength λ can now be expressed as follows:

$$dA_{t,\lambda} = -\frac{\partial I_\lambda}{\partial t \cdot I_\lambda}\Delta t = \Delta l \sum_i \epsilon_{i,\lambda} \cdot c_i, \tag{5}$$

where the effects of all the different absorbents (hemoglobin types) having different absorption coefficients and concentrations are summed together. The differential can also be expressed in terms of the detected light intensity change:

$$dA_{t,\lambda} = -\frac{\Delta I}{I} \cong \frac{I_{AC,\lambda}}{I_{DC,\lambda}}, \tag{6}$$

where $I_{AC,\lambda}$ is the time dependent and $I_{DC,\lambda}$ the time independent component of the measured transmission at wavelength λ. Pulse oximeters use this approximation to compare measured absorbances at red (R) and infrared (IR) wavelengths in order to estimate the ratio of oxyhemoglobin and reduced hemoglobin, or more often, the percentage of oxyhemoglobin in total hemoglobin content, denoted $S_\mathrm{p}O_2$. The relation of absorbances to oxygen saturation is shown in equation (9).

$$\frac{dA_R}{dA_{IR}} = \frac{I_{AC,R}/I_{DC,R}}{I_{AC,IR}/I_{DC,IR}} \tag{7}$$

$$= \frac{(\epsilon_{O_2Hb,R} \cdot c_{O_2Hb} + \epsilon_{RHb,R} \cdot (1 - c_{O_2Hb}))\Delta l}{(\epsilon_{O_2Hb,IR} \cdot c_{O_2Hb} + \epsilon_{RHb,IR} \cdot (1 - c_{O_2Hb}))\Delta l} \tag{8}$$

$$= \frac{S_pO_2 \cdot \epsilon_{O_2Hb,R} + (1 - S_pO_2) \cdot \epsilon_{RHb,R}}{S_pO_2 \cdot \epsilon_{O_2Hb,IR} + (1 - S_pO_2) \cdot \epsilon_{RHb,IR}} \tag{9}$$

The equation (9) clearly shows that the simplified ideal model assumes that the only absorbents present in arterial blood are oxyhemoglobin and reduced hemoglobin. In most cases it poses no problem since the normal levels of carboxy- and methemoglobins are rather low [5], but some drugs and dyes in the circulation may have a big, unwanted effect on the measurement. The ideal theory can be generalized for n wavelengths and m hemoglobin types (n being greater than or equal to m) to improve either on the number of substances measured or the accuracy of measurement [13], but it is not in the scope of this thesis.

Although the basis of oximetry is the Beer-Lambert law it can't be directly applied since the law only holds for monochromatic light through homogeneous and isotropic medium with no scattering and no association or dissociation of absorbing molecules. Since photoplethysmography of human tissue clearly doesn't fulfill these boundary conditions, empirical calibration is needed. [5, 17]

3.2 S_pO_2 Measurement

Arterial blood oxygen saturation measured by pulse oximetry (S_pO_2) is an estimate of the functional arterial oxygen saturation S_aO_2, which is the actual percentage of oxyhemoglobin of all the functional hemoglobin in the blood.

$$S_aO_{2(func)} = \frac{O_2Hb}{O_2Hb + RHb} \cdot 100\% \tag{10}$$

Figure 8: *A typical S_pO_2 measurement setup.*

A typical pulse oximeter measurement setup is shown in figure 8. The sensor has the two LEDs on one side of a fingertip and a photodetector on the other

Figure 9: *A typical measurement cycle of a pulse oximeter.*

side, and by pulsing the LEDs as indicated in figure 9 with a sufficient frequency, both of the photoplethysmographic signals can be obtained concurrently from the gathered data points. The duty cycle of the LEDs is usually between 5-10% to allow for bigger peak currents without overheating the sensor – as the sensor is used continuously in contact with skin, the temperature shouldn't rise much over normal body temperature [18].

The measurements are processed with a suitable algorithm detecting and filtering out the most common disturbances explained in section 3.3 and used to calculate the S_pO_2 value by comparing their normalized differential absorptions given in equation (6). This produces a ratio R, also known as a *ratio of ratios*:

$$R = \frac{I_{AC,R}/I_{DC,R}}{I_{AC,IR}/I_{DC,IR}}. \tag{11}$$

Equation (9) states that this ratio depends only on the blood oxygen saturation – due to its relative nature it's unaffected by tissue thickness, skin pigmentation, blood volume, cardiac output, semiconductor nonlinearities or other variables that directly affect the absolute values of both of the pleth signals. The relationship between oxygen saturation and R can be derived from the absorption spectra of the hemoglobin species to some extent using the ideal model, but for more accurate real-life measurements pulse oximeters use empirically gathered calibration data. The data is usually collected using a more accurate reference device, a co-oximeter, which requires a blood sample to be drawn from the subject. [5]

Modern pulse oximeters calculate other parameters as well in addition to S_pO_2 from the same measurement: heart rate, perfusion index and plethysmographic variability index with a visualization of the plethysmographic waveform provide an excellent tool for the doctor to estimate the patient's state. [19, 20]

3.3 Limitations of Pulse Oximetry

It's to be noted that the S_pO_2 figure is only relative and doesn't take the total amount of hemoglobin into account – it doesn't tell the observer anything about the blood's total oxygen content. None the less, it's a good indicator for any possible disturbances in the respiratory and cardiovascular systems and in many cases serves as an early warning system for various critical conditions. Still, even though an ICU standard, pulse oximetry has some other drawbacks and limitations that have to be taken into account when assessing its reliability in clinical use and to avoid misinterpretation of measurements. They range from technical issues such as electromagnetic and physical interference to physiological limitations affecting the optical properties of the tissue, and some of them are discussed here.

3.3.1 Ambient Light

Probably the most obvious issue with oximetry is the ambient light that inevitably will find its way to the photodetector and is summed up in the measurement signal: if it contains some harmonic frequencies of the measurement cycle it may cause significant DC error and in any case add a lot of noise. Especially fluorescent and xenon lights in operating rooms have been known to cause both falsely normal and abnormally high readings even with the probe off patient. The effect of ambient light can be diminished physically by covering the probe with an opaque shell and by using measurement frequencies the harmonics of which don't coincide with the harmonics of the electric grid frequency. [21]

While the actions above are essential in limiting the ambient noise, a more sophisticated method of diminishing the effect exists. If the measurement cycle is short enough, by measuring the ambient level associated to each LED pulse (figure 10) and subtracting the value from the result one can obtain a rather ambient-free result with only adding the noise of another sampling and conversion. The frequency response depends on the delay between the ambient and LED pulse measurements but in any case noise attenuation is of type 1/f. Considering that the bandwidth of interest is usually much lower than the sampling frequency and that of line frequency, this method blocks most of the noise on that band.

3.3.2 Patient Related Sources of Noise

Another significant error source in pulse oximetry are motion artifacts. Given that the magnitude of the pulsatile signal is only percents of the total light transmission, any motion of the patient causing changes in local blood pressures and possibly sensor movement in respect to the tissue may greatly disturb the measurement. Caused by shivering, seizures or voluntary movements, the S_pO_2 algorithm may not detect the motion artifacts if their waveform resembles a normal plethysmographic signal which usually will lead to false readings and possibly an alarm. Modern oximeters utilize advanced signal processing methods to improve their accuracy even during motion artifacts. [5, 22]

Figure 10: *A typical S_pO_2 sampling sequence with ambient removal.*

A source for error that is especially bothersome in intensive care is the effect of low peripheral blood perfusion which can be caused by e.g. hypothermia, low cardiac output, loss of blood and symphathetic nervous activity, all of which can be a reason for intensive care in the first place. When the pulsatile signal intensity decreases it becomes exceedingly difficult for the measurement circuit to detect the plethysmographic signal from background noise. Pulse oximeters generally aren't able to operate if perfusion is very low, meaning an AC amplitude of 0.1% of the total signal level or less, and produce an alarm instead.

Since most pulse oximeters are calibrated for normal, healthy people and only have two wavelengths, they have to assume that dyshemoglobin levels are sufficiently low. In some cases though, for example in carbon monoxide poisoning or methemoglobinemia, the patient's dyshemoglobin levels can rise dangerously high, greatly diminishing the oxygen carrying capacity of the blood. The spectral absorbance of carboxyhemoglobin greatly resembles the one of oxyhemoglobin, resulting in falsely high readings when carboxyhemoglobin concentration is elevated [23]. Small amounts of methemoglobin tend to drive the oximeter reading falsely high, but with levels of over 20 percent the reading settles around 85% [24]. In addition, some drugs cause methemoglobinemia as a side effect which means that when administering them it should be noted that the pulse oximeter calibration isn't valid anymore [5].

Also dyes and drugs, or any substances, for that matter, in the blood that have an uneven absorption spectrum in the pulse oximetry range can affect the reading. The standard intravenous imaging dyes methylene blue, indocyanine green and indigo carmine have significant absorptions at the 660 nm wavelength but only minor absorptions at 940 nm [25, 26]. Thus, the use of these substances falsely decreases S_pO_2 readings.

To summarize, it's extremely important for the physician to be aware of the

various limitations of pulse oximetry and to apply another measurement technology when there's a known risk of false readings. [5, 27]

3.4 Conventional System Design

Pulse oximetry solutions usually resemble a configuration such as in figure 11: the system is controlled by a microprocessor which has inputs and outputs for all the peripherals and provides timing and operating levels for the analog measurement circuit, also known as the analog front end (*AFE*). The AFE in turn provides the processor with measurements through the high-precision ADC for post-processing. The front end is usually implemented with a number of discrete components and integrated circuits, the blocks in the diagram roughly corresponding to the final setup. To be able to operate on a wide dynamic range the front end must have several processor-selectable LED current options and amplifier gain settings.

Figure 11: *A typical block diagram of a pulse oximeter showing the Analog Front End, the Processor and some peripherals. [28]*

The analog front end can be divided further into two blocks: the LED driver and the receiver. The driver can be implemented as a *common cathode* circuit where each LED has its dedicated anode wire and the cathodes are connected to a shared ground, or a *back-to-back* circuit where the LEDs are connected to the same wires but with reversed polarities and are driven by an H-bridge – this has the advantage of needing only two wires from the circuit board to the probe but also the disadvantage of the voltage drop of the added switch in the signal path. Both configurations are shown in figure 12. The driver also includes a transconductance amplifier providing a controlled current proportional to its input voltage from the DAC, eliminating the effect of variable resistances in different probes and wires.

The basic receiver configuration, in addition to the photodetector, includes a transimpedance amplifier to convert the photodetector current into a voltage signal,

Figure 12: *Different LED configurations, using a different number of wires and a different driver.*

a low-pass filter, a sample-and-hold circuit and a high-precision A/D converter as illustrated in figure 13. Typically the ADC has a precision of at least 18 bits, often even more. To take full advantage of the ADC, the analog front end must be designed to have as good a signal-to-noise ratio (SNR) as possible, though; usually this means that the operational amplifier component must be of high quality and with extremely stable reference voltages. [5]

Figure 13: *A simplified example of a typical pulse oximeter receiver. The separation of AC and DC signal paths is optional and is recommended only in the case that the ADC has a low number of bits. [5]*

Considering the low signal levels, noise is an important factor when designing the front end, and ensuring a signal-to-noise ratio (SNR) as high as possible is vital for the device's operation in more challenging situations. When designing a system like this there's bound to be some trade-offs between performance, power and price, some of which are discussed next.

In the measurement there's a strong relationship between LED current, pulse width and receiver gain. Ideally, the emitted light would be as bright and continuous as possible for the receiver to get the strongest possible signal, but in reality the LED drive power usage should be kept as low as possible for both battery life and probe temperature reasons. Therefore the multi-parameter optimization goal is to minimize LED power while maintaining such a signal-to-noise ratio that the measurement is reliable in all the designed use cases.

The noise produced by the LED driver doesn't account much to the overall system performance – after all, the signal is strong while thermal noise is rather constant. The main sources for electrical noise in the system indeed are in the receiver side, mainly the photodiode itself, its cabling and the trans-impedance

amplifier. Because of the as-low-as-possible emitted light intensity, the photodiode may exhibit noticeable shot noise in addition to thermal and 1/f noise present in all conductors. On top of that, shortening the LED pulse increases the bandwidth demand of the receiver. Since (white) noise energy is directly proportional to the bandwidth, this all leads to the fact that there's a big trade-off between LED power and receiver noise when controlling both the pulse intensity and the duty factor. [29, 30]

Short pulse length can be an upside as well, though: the shorter the pulse, the more closely the actual measurement and the ambient measurement can be packed, better eliminating ambient noise. By using a higher pulse repetition frequency the measurements can be averaged and decimated down to the target sample frequency, decreasing total noise.

4 Noise Characterization

The most important factor of the system is its noise behavior. It directly poses limits on the operating conditions within which the device is accurate enough and thus defines its usability and reliability in the most difficult and life-threatening situations. As no system is perfect, this chapter focuses on defining an acceptable noise level based on the specification, system design and the noise performance of the algorithm used.

4.1 Noise Requirements

The ISO 80601-2-61 standard defines a baseline of performance requirements for S_pO_2 monitoring that GE devices should meet [18], but more importantly, competitors' devices claim to achieve even better performance. Masimo and Covidien (Nellcor) both report an RMS overall error of 2 percentage points in the S_pO_2 reading with IR modulation as low as 0.03% [31], which means that it's good business for GE to top that figure. Therefore the goal is to stay below 2 percentage points of error down to IR modulation of 0.02%. This imposes a strict requirement for the system's noise behavior since a signal that weak can easily be lost in the noise floor, depending on the algorithm used.

The simplest algorithm to use for calculating R (equation 11) is the peak-to-peak algorithm: the signal is analyzed and the values for I_{AC} and I_{DC} are found by recording the maximum, minimum and mean values of the signals. In this case the peak-to-peak noise present in the full frequency band of interest affects the measurement directly, thus skewing the S_pO_2 result. As the pleth signal is usually in the range of 0.5-20 Hz, the dominating noise type can be either white or 1/f.

The formulation of the noise requirement for the system can be started with deriving the equation (11) and assuming that the noises in the two channels sum up in a root-mean-square manner:

$$\begin{cases} \frac{dR}{dI_{AC,R}} &= \frac{I_{DC,IR}}{I_{AC,IR} \cdot I_{DC_R}} \\ \frac{dR}{dI_{AC,IR}} &= -\frac{I_{AC,R} \cdot I_{DC,IR}}{I_{AC,IR}^2 \cdot I_{DC,R}} \\ \Delta R &= \sqrt{(I_{n,R} \cdot \frac{dR}{dI_{AC_R}})^2 + (I_{n,IR} \cdot \frac{dR}{dI_{AC,IR}})^2} \end{cases} \tag{12}$$
$$\rightarrow \Delta R = \sqrt{I_{n,R}^2 + (I_{n,IR} \cdot \frac{I_{AC,R}}{I_{AC,IR}})^2} \cdot \frac{I_{DC,IR}}{I_{AC,IR} \cdot I_{DC,R}}$$

By defining the signal modulation ratios and assuming that the signals can be controlled so that they are at the same DC level it can be concluded that

$$\begin{cases} m &= \frac{I_{AC}}{I_{DC}} \\ m_R &= R \cdot m_{IR} \\ I_{DC,R} &= I_{DC,IR} = I_{DC} \end{cases}$$

$$\Delta R = \sqrt{I_{n,R}^2 + (I_{n,IR} \cdot R)^2} \cdot \frac{1}{I_{AC,IR}} \tag{13}$$

$$\Delta R = \frac{\sqrt{I_{n,R}^2 + (I_{n,IR} \cdot R)^2}}{I_{DC} \cdot m_{IR}}$$

Equation 13 states that the error in R imposed by noise is directly proportional to the noise level and inversely proportional to the signal level and modulation ratio. The specification determines the minimum modulation ratio but the optimal signal level is defined by the system's dynamic behavior; usually the signal is kept in the middle of the ADC's dynamic range, leaving room for detecting motion and other artifacts, but the better the system the closer the signal can be kept to the high limit of the range.

For the sake of simplification it's assumed that the noise magnitude is the same for each channel, which is also true on average. Therefore the equation reduces itself to a form that will be used in further calculations:

$$\Delta R = \sqrt{1 + R^2} \cdot \frac{I_{n,pp}}{I_{DC} \cdot m_{IR}}. \tag{14}$$

As explained in section 3, R maps to an S_pO_2 reading with a non-linear relation. Calibration data is used for this mapping but usually the relationship is the form of an equation of 2nd degree, and said equation can also be used to find the relation between the error in R and the error in S_pO_2 :

$$\begin{aligned} S_pO_2(R) &= aR^2 + bR + c \\ R(S_pO_2) &= \frac{-b - \sqrt{b^2 - 4a(c - S_pO_2)}}{2a} \end{aligned}$$

$$\Delta R(S_pO_2, \Delta S_pO_2) = R(S_pO_2 + \Delta S_pO_2) - R(S_pO_2) \tag{15}$$

$$\Delta R(S_pO_2, \Delta S_pO_2) = \frac{\sqrt{b^2 - 4a(c - S_pO_2)} - \sqrt{b^2 - 4a(c - S_pO_2 - \Delta S_pO_2)}}{2a}$$

By combining equations (14) and (15), fixing S_pO_2 tolerance and solving the equation in respect to I_n a relationship is established between the performance specification and allowed noise level:

$$\begin{aligned} I_n(S_pO_2) &= I_{DC} \cdot m_{IR} \cdot \frac{\Delta R(S_pO_2, \Delta S_pO_2)}{\sqrt{1 + R^2(S_pO_2)}} \\ I_n(S_pO_2) &= I_{DC} \cdot m_{IR} \cdot \frac{\sqrt{b^2 - 4a(c - S_pO_2)} - \sqrt{b^2 - 4a(c - S_pO_2 - \Delta S_pO_2)}}{\sqrt{4a^2 - 4a(c - S_pO_2) + 2b^2 + 2b\sqrt{b^2 - 4a(c - S_pO_2)}}} \end{aligned} \tag{16}$$

The overall noise tolerance of the system is the minimum of the function above. The function solved with values defined in table 1 is plotted in figure 14. It's to

be noted, though, that the tolerance figure includes all calibration errors, motion and respiratory artifacts and other sources of error – therefore the signal path itself should introduce even less noise for the system to fulfill the requirements in normal operating conditions. Based on data gathered from previous GE oximeter designs it's estimated that most, but not all, of the total error is due to additive noise in the signal path and the rest is from other sources; if the allowed 1-σ tolerance in the S_pO_2 value due to signal path noise is defined to be 1 %-point, the required signal-to-noise ratio calculated using the same method is approximately 127 dB. Assuming white spectrum, the peak-to-peak noise is converted to RMS noise by dividing by 6.6 for the calculation of SNR.

Table 1: *Example calibration values and performance specification constants*

Item	**Symbol**	**Value**
Calibration coefficient	a	-6.68
Calibration coefficient	b	-19.9
Calibration coefficient	c	112
IR Modulation Ratio	m_{IR}	0.0002
Signal Level	I_{DC}	5 μA
Output tolerance	ΔS_pO_2	$\pm$1 %-point
Output range	S_pO_2	70–100 %
Pleth power distribution coefficient	α	0.3
Noise power distribution coefficient	β	$\frac{1}{64}$

Figure 14: *The system's maximum noise level as a function of S_pO_2 reading according to equation 16 and table 1.*

4.2 S_pO_2 Algorithm and Noise

As mentioned previously, the peak-to-peak algorithm in time domain is the simplest one to implement but also the most prone to be disturbed by noise. Fortunately there are alternatives, the more advanced taking advantage of the rhythmic nature of the plethysmographic signal and working in frequency domain.

The frequency domain approach used by GE periodically processes a 5-second window of the signal by performing a Fast Fourier Transform (FFT) on it and seeking the strongest frequency spike to act as the AC signal, similarly to [32]. The benefit of this approach is that since most of the pleth signal's energy is focused on the fundamental frequency it captures the signal properties quite well but is only affected by noise on that specific frequency. This means that most of the white or pink noise present in the system goes unnoticed – the actual advantage gained depends on the frequency step of the FFT and the relationship between noise spectrum and cardiac frequency but effective noise can usually be reduced by a noticeable factor compared to algorithms working in time domain.

Figure 15: *The power spectrum of a typical strong plethysmographic signal showing the fundamental cardiac frequency and its harmonics.*

Figure 15 shows the power spectrum of a typical strong plethysmographic signal windowed to 10 seconds. It's clearly seen that the fundamental cardiac frequency and its harmonics are the dominant components and raise well above any noise levels. The powers of the fundamental frequencies in both channels can directly be divided with the zero-hertz powers and each other to calculate R, α denoting the portion of pleth signal power focused on the fundamental frequency:

$$\begin{cases} R = \frac{m_R}{m_{IR}} = \sqrt{\frac{\frac{P_{f,R}}{P_{0,R}}}{\frac{P_{f,IR}}{P_{0,IR}}}} \\ X_f = \left|\sum_{n=0}^{N-1} x_n e^{-i2\pi \frac{f}{f_s}\frac{n}{N}}\right| \approx \frac{N}{2}\sqrt{\alpha} I_{AC} \\ P_f = X_f^2 \approx \frac{N^2}{4}\alpha I_{AC}^2 \\ P_0 = P_{0,R} = P_{0,IR} = N^2 I_{DC}^2 \end{cases} \tag{17}$$

$$\rightarrow R = \sqrt{\frac{X_{f,R}^2}{X_{f,IR}^2}} = \frac{X_{f,R}}{X_{f,IR}} \tag{18}$$

The square root is necessary to reduce the ratio of powers to a ratio of amplitudes. Alternatively, the relation between S_pO_2 and the calculated ratio could be modified accordingly. Further on, the equation can be derived like done in equation (13) to formulate the noise requirement, taking into account the noise reduction coefficient β achieved from the FFT and assuming that the noises in the two channels will add up in RMS fashion:

$$\begin{cases} \Delta X_f = \frac{N}{2} \cdot \sqrt{\beta} \cdot I_n \\ \frac{dR}{dX_{f,R}} = \frac{1}{X_{f,IR}} \\ \frac{dR}{dX_{f,IR}} = -\frac{X_{f,R}}{X_{f,IR}^2} = -\frac{R}{X_{f,IR}} \\ \Delta R(\Delta X_f) = \sqrt{(\Delta X_f \cdot \frac{dR}{dX_{f,R}})^2 + (\Delta X_f \cdot \frac{dR}{dX_{f,IR}})^2} \end{cases} \tag{19}$$

$$\begin{aligned} \rightarrow \Delta R &= \Delta X_f \sqrt{\frac{1}{X_{f,IR}^2} + \frac{R^2}{X_{f,IR}^2}} \\ &= \frac{\Delta X_f}{X_{f,IR}} \cdot \sqrt{1+R^2} \\ &= \frac{2N\sqrt{\beta} I_n}{2N\sqrt{\alpha} I_{AC,IR}} \cdot \sqrt{1+R^2} \\ \Delta R &= \sqrt{\frac{\beta}{\alpha}} \cdot \frac{I_n}{I_{DC} \cdot m_{IR}} \cdot \sqrt{1+R^2} \end{aligned} \tag{20}$$

$$\rightarrow I_n(S_pO_2) = \sqrt{\frac{\alpha}{\beta}} \cdot I_{DC} \cdot m_{IR} \cdot \frac{\Delta R(S_pO_2)}{\sqrt{1+R(S_pO_2)^2}} \tag{21}$$

Using equation (15) for R and ΔR and parameter values from table 1, the noise requirement formulated by equation (21) can be plotted. The results are shown in figure 16 – using a 64-point FFT, they show a signal-to-noise ratio requirement significantly (30 dB) lower than when using the peak-to-peak algorithm.

4.3 Timing and Channel Noise Correlation

The scenario portrayed in the previous section assumes that the measurement noises present in the different channels drive R towards the same direction instead of countering each other. It's to be noted, though, that as a single receiver chain is used to

Figure 16: *Acceptable system noise level as a function of S_pO_2 reading when using an algorithm that's based on a 64-point FFT and values from table 1.*

measure all four channels (red, infrared, red ambient, infrared ambient) it's probable that most of the noise is common for them, and equation (13) shows that the more correlated the channel noises are the smaller the effect on R is in typical operating conditions.

A feature that helps to reduce uncorrelated noise is oversampling. The sampling frequency can be anywhere between 100 Hz and 1000 Hz, the output filtered and downsampled to the target sample rate, usually 40-100 Hz. When N samples of a DC signal are summed together the result is N times larger but the uncorrelated noise only increases by a factor of $\sqrt{N}$, causing the total signal-to-noise ratio to also increase by $\sqrt{N}$. This is why all noise in this thesis is examined in the target bandwidth of 0.5-20 Hz without taking the actual Nyquist frequency of the raw signal into account.

4.4 Noise Sources

If the system is designed optimally there's no single big noise source in the system that could be directly pinpointed but instead every subsystem in the signal chain adds its own contribution into the total system noise. Most of this is plain thermal noise found in all conductors but each subsystem also exhibits some special behavior that should be taken into account in the design and verification.

4.4.1 LED Current Regulator

The transmitter, or LED drive, regulates the pulsed current directed into the LEDs. Typically the control reference is given by an 8-bit DAC which transfers a digital value into a reference voltage that guides the current regulator. Now, the important feature of the DAC isn't the resolution it provides (8 bits is well enough) but the

repeatability of the conversion result – it is imperative that two current pulses of same reference setting are regulated with the same reference voltage since all variation between the pulses will directly translate into variation between measured samples. For this same reason the noise of the band gap providing a reference for the DAC has to be as small as possible.

All in all, with current technology it's reasonably easy to build a cost-effective LED drive that has a signal-to-noise ratio of 115 dB, which is the design specification of the transmitter in the new design. The 115 dB specification ensures that the transmitter noise is well below receiver noise and can often be treated as non-existent.

4.4.2 Photodetector

Noise in a photodiode is primarily due to shot noise – the random generation of carriers within the P-N junction also yields random current. Negatively biasing the photodiode increases the response speed and sensitivity of the detector but also increases noise [33], due to which GE uses non-biased detectors. In general as the detector is the source of signal in the receiver chain its noise behavior defines the minimum detectable power of the whole system.

4.4.3 Trans-Impedance Amplifier

A trans-impedance amplifier transforms a current signal into a voltage one. It is usually implemented with an operational amplifier with the voltage over a resistor the current flows through as the input. Even though the system's input is differential, due to the length of the sensor cable and noisy environment it is still possible that large induced voltages are present as a common-mode disturbance. Due to this it is important that the op-amp selected has a good common-mode rejection ratio (CMRR) in addition to low overall noise. For the higher-end amplifiers of National Semiconductor typical CMRR values are in the range of 130 dB and input noise ca. 3.3 $nV/\sqrt{Hz}$ [34].

As [35] states, the power of a noise signal isn't changed by sampling; therefore when calculating the SNR of the op-amp, the full bandwidth, which in turn is defined by sampling rate, must be taken into account. For a sampling rate of 625 Hz the SNR of the part above for a signal of 0.5 V would be in the range of 135 dB which is well above the specification of the whole system. In any case, due to the feedback circuit the output noise of the operational amplifier usually has a linear relationship to its gain, namely the feedback resistor.

4.4.4 Sample-and-Hold

A sample-and-hold block is most commonly implemented as a switched capacitor circuit working in two phases: during sampling phase the input is switched in to charge the sampling capacitor and during hold phase the voltage of the capacitor is buffered to output. Therefore the effective noise of the circuit can be broken into sampling noise and hold-time continuous noise as well. [36]

As the hold-time noise is usually of little significance, only sampling noise is handled here. The primary source for it is that the sampling circuit's thermal noise introduces a random component in the sampled signal: the sampling capacitor will hold the voltage that the input had when the switch was opened. As the high-pass filtering properties of the capacitor are related to its capacitance, the sampling noise can be formulated as [36]

$$V_{nRMS} = \sqrt{\frac{k_B T}{C}}. \tag{22}$$

This leads to the fact that careful thought must be put into selecting the capacitor: a small capacitor offers a fast response allowing for short sampling times but introduces more noise than a bigger one.

4.4.5 A/D Conversion

Most A/D converters tend to be sigma-delta types. They operate at a much higher frequency than the actual sampling and conversion frequency and use a feedback loop comparing the latest result to the input signal level [37]. For accurate operation the converter needs a stable reference voltage, an accurate clock and a noise-free input. As all analog-to-digital conversions show quantization noise a completely noise-free conversion is impossible; the relative quantization noise in signals close to zero could be diminished by utilizing a logarithmic conversion scale but due to practical reasons concerning signal post-processing it is rarely used.

4.4.6 Ambient Light

Although the measurement site can be shielded with an opaque shell covering the sensor, it's still highly probable that some ambient light still finds its way to the photodetector. This can be a problem especially in operating room conditions where high intensity illumination is required. The noise caused by ambient light is typically double line frequency (100 or 120 Hz) noise with a DC component, thus disturbing both the AC and the DC measurement. This is why the ambient level is sampled as well and subtracted from the red and infrared measurements. In addition to removing the ambient effect the subtraction also removes other correlated low frequency noise from the signal.

5 The New Pulse Oximetry Measurement Circuit

In an attempt to produce a small, low-power pulse oximeter, a new analog front-end (*"AFE"*) was developed and microcontroller software written to control it. The emphasis was in building a complete measurement platform able to provide any back-end supporting the communication protocol with measurements with as little need for customization or configuration as possible – a kind of full independent measurement system that has a minimal external interface enabling easy integration into practically any host. Also, the measurement quality should be as good or better than in the current designs while minimizing power consumption. Wireless sensors are especially interesting future applications of this design, the block diagram of which is shown in figure 17.

Figure 17: *The block diagram of the new system. The system doesn't take any stand on the selection of the back-end processor – it can be a microcontroller, a DSP or even a PC.*

5.1 Microcontroller

The microcontroller used is TI MSP430F5529 [38], an ultra-low power RISC processor with a number of peripheral modules. The processor is in the higher end of the MSP430 family with several DMA channels, four timers and many communication modules, yet still doesn't have the processing power of e.g. ARM processors. It is still powerful enough to perform well as a measurement module for a host processor or even as a stand-alone unit with a less advanced signal processing algorithm using only a minimal amount of electrical power.

In addition to a number of general purpose I/O ports and a USB module, the microcontroller has two USCI modules for communicating with a host processor or other peripherals. One of them is dedicated for communicating with the AFE's analog-to-digital converter via SPI. In the developed application the other one is used for host communication via UART yet possible other solutions include, but aren't limited to, operating a display driver for displaying results or sending the measurement data using an external radio module.

5.2 Analog Front-End

The analog front-end consists of a current-regulating transmitter, a receiver with multiple gain stages and a 22-bit ADC. It is capable of performing hardware diagnostic tests on the probe, checking for short and open circuits on all the lead combinations. It supports two transmit channels and four measurements per cycle, measuring both the "LED ON" value and the ambient value for both channels. LED current and receiver gain are individually selectable for both channels, enabling truly independent control for both of them.

The key to the operation of the AFE is timing. A number of control signals are produced for all the components of the AFE, guiding their operation precisely. The signals are "enabling" signals as opposed to triggering signals: For example, from the internal timer's perspective the signal *RED ON* is defined as the interval between a starting counter value and an ending counter value and is set high for that period of time. It is then used so that current is fed into the red LED when said signal is high. The same applies for other timing signals (LED ON, SAMPLE, CONVERT). It's up to the microcontroller software to set the compare registers' values so that the possibly conflicting signals don't overlap.

The transmitter (figure 18) has two active parts: a current controller that gets its reference from an 8-bit D/A converter, and an H-bridge for switching the current on and off for each LED in configurations shown in figure 12. In short, it provides precisely timed pulses with constant currents without any crosstalk between the two channels. As the power supply is current limited and the drive capacitor not infinite the pulses have to be separated enough, though, or otherwise the latter might suffer from the temporary voltage drop caused by the former when using high LED currents.

Figure 18: *A block diagram of the AFE's transmitter unit showing the H-bridge, the current controller and the control signals.*

The receiver is a bit more complicated (figure 19), consisting of an amplifier with selectable gain and filtering properties, four sampling units and a buffered A/D converter. The gain can be set by selecting a value for the feedback resistor R_f out of the values available, ranging from 10 kΩ to 1 MΩ. The amplifier's time

constant and thus its low-pass bandwidth is defined by the combination of R_f and the feedback capacitor C_f, implying that the two should be defined as pairs. The cutoff frequency is also coupled with the LED pulse length: the shorter the pulse the higher the amplifier's bandwidth must be. This imposes another optimization problem since energy-and-signal-strength-wise a shorter pulse with a higher amplitude is preferred to a longer pulse with a lower one, but increasing the filter bandwidth to allow the shorter pulse also increases the relative amount of noise passed through.

Figure 19: *A block diagram of the AFE's receiver unit, showing how the various signals control its operation.*

5.3 Advantages and Drawbacks

The most obvious advantage of the setup is its reduced power consumption since it's the first GE design to specifically take that into account. By implementing the measurement control with a low-power microcontroller and buffering the samples the back-end processor can remain in sleep mode for most of the time, only waking up to handle new measurements; also designing the system with power consumption in mind from the beginning allows for a more optimized design. The power used for front-end processing alone can be reduced to 1 mW and the power used by the AFE, excluding LED drive power, is in the range of 6 mW. Compared to the average power consumption of a suitable ARM microcontroller (Atmel SAM3S, 90mW) [39], not to mention a conventional AFE, the power reduction is significant.

The other major upside in the design is its mechanical simplicity: in addition to being small, once the module is completed it will be extremely easy to design a range of platforms with different peripherals for it. Also the assembly process is simpler and cheaper due to the reduced number of components. In short, the design allows for a device that is more power-efficient and in many cases cheaper to manufacture without compromising the accuracy of the measurement.

A drawback in the solution is that it leaves little room for future development as it is heavily optimized for current design specifications. Therefore scaling it up for more wavelengths or more processing power is out of the question without significant existing market demand.

5.4 Special Considerations for Verification

The special design of this chip makes its verification process and performance tests a bit more difficult than usual: as the circuitry is very tightly packed and well shielded it is practically impossible to measure signals within the receiver chain without affecting performance. This calls for a new statistical approach for assessing performance, a kind of regression analysis, which is the main emphasis of this thesis and will be thoroughly explained in sections 6 and 7.

6 Design Verification Process

The development of the AFE hardware was separated from the software controlling it, in practice meaning that the verification of the hardware design by measuring its performance in different situations was the software team's (for the most part, the author's) responsibility, although the hardware team did provide some support in interpreting the results.

The verification was begun by analyzing the very first prototypes of the AFE, put together on the same board with a microcontroller and a power supply, and continued with the second round of prototypes where the microcontroller and the AFE were more tightly bound and shielded. The aim of the verification process was to determine the system's operating limits and properties and to analyze the noise behavior of individual subsystems and the system as a whole with different settings.

The verification process was made difficult by the fact that the AFE has such a wide range of options – to find the optimal set of timings and other control values was no easy task and took a lot of effort and analyzing. In the following chapters the methods applied to the task are explained.

6.1 Regression Analysis

Regression analysis is a collection of statistical methods for modeling and analyzing a system, the focus being on identifying system variables and/or parameters and their relationships [40]. In this particular case regression analysis can be used to estimate the performance of the different subsystems by carefully selecting the dependent variable and varying one as carefully picked independent variable (i.e. a system parameter) at a time.

6.2 Methodology Used

The fundamental issue with analyzing the performance of the chip is that the analyzing equipment and wiring should be much less noisy than the system to be analyzed in order to get any reliable and quantifiable results. As the noise levels in question are extremely small it posed some restrictions on how the validation could be done – therefore it was decided to design a set of tests that could be done using the system itself and that would provide data about both the system as a whole and about individual subsystems.

The tests were made to be a set of measurement series, in each of which only one measurement parameter was changed. By combining data from these measurements it was possible to determine how each of the subsystems performed with different settings using regression analysis and to find the optimal operating modes for different use cases using only the AFE's transmitter as the stimulus and the AFE's receiver as the data collector.

The key to the making up of the tests is to know the system completely. Many of the configurable parameters in the measurement are intertwined, rendering isolated changes in one of them pointless unless one knows how it really will affect the

system. An example of such interconnections is LED pulse length: not only does it affect the required sampling time and resulting sampling noise, but also the low-pass filter composed of the RC feedback circuit must be tuned so that the corner frequency is sufficient for passing the pulse without too much distortion. Therefore the measurement parameters weren't always atomic values but combinations of them previously identified as isolated, correlated sets of values. In short, a lot of effort was put into analyzing the dependencies between the system variables and isolating independent combined parameters.

6.3 Embedded Software Design

The software used within the microcontroller was designed and implemented so that it would both support the verification process and eventually end up as the final product software. This required a kind of agile development method based on Scrum [41] where each iteration produced a usable product with more functional features than the previous one, the order of development highly guided by the progress of the verification process. The verification required a number of features not needed in the final product which meant that they had to be well isolated from the core program, dependencies being strictly unidirectional. The embedded software was written in Embedded C++, using IAR's compiler and linker [42].

In the evaluation phase the software had two key features: as all control and analysis was done externally it had to be able to fetch the measurements from the ADC and send them through a serial link to a PC and it had to be able to receive commands from said link and set AFE control values accordingly. This meant that the very first pieces of software implemented were the drivers and higher-level manager classes of both the SPI interface for the ADC and the UART interface for PC communication, naturally using the communication protocol selected for the final product. Gradually the number of features was increased, starting from calculating some combinations of control values based on input and moving on to handling the diagnostics and automatically setting all the control values based on measured signal level and desired power mode. The development paradigm supported simultaneous verification and software development very well and proved to be successful throughout the project.

Figure 20 shows the class structure of the software. It can be seen that the communication interfaces are separated from the rest of the code, providing a platform that doesn't take any position on its usage. All the received commands are handled in the main program – in fact, all the validation-only code is confined in the 'Assp' class. Also, the communication drivers tightly bound to hardware are separated from the manager classes to provide sufficient abstraction and thus more portable code.

The program is based on interrupts raising flags that trigger actions in the main program. For example, the end of an A/D conversion is indicated by raising a flag in an interrupt service routine. The main program detects it and executes the measurement fetching subroutine when it has finished any ongoing task. This approach makes sure that the response time is always rather fast but also that

Figure 20: *The structure of the embedded software of the MSP430 microcontroller.*

no ongoing task gets blocked by overly processor-intensive interrupt handlers. On the other hand, using hardware-dependent interrupts makes automated testing of the code difficult and impractical; because of this several manually-run tests were written to ensure code integrity.

6.4 PC Software Design

The analysis software, shown in figure 21, was built on top of Matlab using its proprietary scripting language and user interface designer. The goal of the software was to provide a tool for setting the AFE parameters and evaluating the result online, and also for capturing data for offline analysis. The user interface shows the output and its power spectrum as graphs, the AFE's control values as a list and provides an interface for changing any or all of them.

6.5 Critical Tests and Derived Parameters

After being established that all the features of the AFE work as intended, the most important property of the system to evaluate is its noise performance as indicated in chapter 4, and in the case of not immediately reaching the target, identifying the dominant noise source. Methods for this include plotting measured system noise as functions of receiver gain, transmitter current, pulse length, pulse repetition frequency, and other variables. From the results it's possible to deduce with reasonable accuracy the amount of noise each subsystem contributes to the final figure by fitting a theoretical model on the measurements.

The components producing noise in the signal chain can be listed as follows:

- Transmitter noise (current variability from one pulse to another, timing jitter)
- Photodiode noise (shot noise) and settling time

Figure 21: *The PC software used to remotely control the measurement system with features for visualizing and processing both the incoming samples and the system's internal state.*

- Noise induced into the photodiode cable leads from the environment and LED leads
- Thermal noise in the conductive path
- Receiver op-amp noise
- Sampling noise
- A/D conversion noise.

Transmitter noise can be identified to some extent by measuring the receiver noise floor without the transmitter and then measuring with the same settings, only this time with transmitter on. Similarly, the effect of the photodiode and the cable can be identified by replacing the sensor with a dummy block. The tests performed are explained more thoroughly in the next chapter but the key to the analysis is to identify the alterable system parameters that affect only the performance of a single subsystem.

6.5.1 Distinguishing Amplifier Noise From Sampling and Conversion Noise

With zero input (photodiode pins connected through a big resistor), it is assumed that all noise in the receiver output is due to suboptimalities in three distinct sub-

systems: the cross-impedance amplifier, the sampling unit and the conversion unit. Since all noise produced before the amplifier stage including the operational amplifier's noise itself gets amplified, with zero signal the amplifier noise is assumed to have a somewhat linear relationship to the gain used. Everything after the amplifier on the other hand should be rather constant with respect to gain, meaning that measuring system noise as a function of gain should result in an estimate of the magnitudes of the effective noises of the individual subsystems.

As said, the sampling and conversion noises are virtually unaffected by receiver gain. The key parameter determining sampling noise is sampling time, the relationship being inverse like the relationship between conversion noise and conversion time as well. Additionally, all the noise components are assumed to be white and uncorrelated, meaning that their magnitudes add into each other in a root-mean-square manner. These assumptions give us a rudimentary model of the noise system of the receiver:

$$\begin{aligned} \sigma_{receiver} &= \sqrt{(a \cdot R_f)^2 + (\tfrac{b}{\tau_s})^2 + (\tfrac{c}{\tau_c})^2} \\ \sigma_{receiver}(R_f) &= \sqrt{(a \cdot R_f)^2 + \sigma_{sc}^2} \end{aligned} \tag{23}$$

If plotted as a function of R_f the result could be something like in figure 22 – The part of the noise not related to R_f can be clearly identified from the point $R_f = 0$, making the estimation of the parameter a an easy task. Similar plot can be drawn for the noise as a function of conversion time, but not for sampling time – sampling time also defines the optimal corner frequency of the amplifier feedback low-pass filter which makes the two connected.

6.5.2 Distinguishing Transmitter Noise From Receiver Noise

In previously examining the receiver only zero input signal was used. That might impose a problem when trying to assess transmitter noise by directly measuring the noise of the system when used as indicated in figure 23 since the receiver might not perform identically with a signal that has a non-zero DC level. Therefore a measurement circuit was devised that would allow measuring the transmitter's noise behavior in DC mode as a function of LED current, illustrated in figure 27. That is not enough, though, as the transmitter's performance must also be examined in pulsating mode.

6.5.3 Receiver Noise with a Dynamic Signal

The big problem in identifying the receiver performance in normal operating conditions is that it's very difficult to produce a pulsed reference input signal small and noiseless enough so that it could be used to measure the receiver's dynamic behavior. As the DC measurements defined earlier don't tell much of the receiver's performance in normal operation, this is both interesting and crucial in assessing the performance of both the receiver and the transmitter: If such a signal is available it can be used to determine the receiver's noise which in turn can be used to calculate the noise component caused by the transmitter in normal operation.

Figure 22: *Estimated system noise according to the model in equation (23) plotted as a function of R_f.*

The main challenge with the reference signal is that its amplitude must be very small to avoid saturating the receiver; the maximum current should be in the range of 0.5-25 μA depending on the receiver gain setting which is a lot to ask from most signal generators, especially as its noise level should be well below the receiver's. Also, to simulate a typical pulse oximetry signal the reference signal should be pulsed and synchronized to the measurement cycle so that the top of the square wave coincides with signal sampling.

Perhaps the most useful input signal for characterizing the receiver only would be a pulsed one which is amplitude modulated with an approximately 0.5-5 Hz (30-300 bpm, normal cardiac range) pure sinusoidal signal. It could be used to measure the receiver's critical characteristics such as noise, distortion, harmonic noise, linearity and phase response by comparing the measured signal to the ideal one.

6.5.4 Transmitter Noise in Normal Operation

The specifications of the transmitter claim that its signal-to-noise ratio is constant throughout the dynamic range. As the noise caused by the receiver is measured in the previous test, it is fairly simple to estimate the effect of the transmitter as a function of LED current with the following equation:

Figure 23: *The setup of the validation. A standard sensor with a light attenuation block is used as the transmitter-receiver coupling device. As the attenuation block is static the output signal should be a DC one, which allows using the output's standard deviation as the primary measurement quality indicator.*

$$\sigma = \sqrt{(k \cdot I_{LED})^2 + \sigma_{Rx}^2}. \tag{24}$$

Again, it is assumed that the different noise components are white and uncorrelated – in actual operation this might not be the case if e.g. noise originating from the power supply is summed up into both the transmitted and the received signal or if there's significant crosstalk between the transmitter and the receiver. For the purposes of testing only the AFE the assumption is enough, though.

7 Performance Analysis

The first prototype of the new AFE was delivered for analysis right after it was assembled, meaning that even the hardware team didn't have any valid data about its performance at the time. Once it was up and running it was put to testing to assess its suitability for the upcoming pulse oximetry designs.

7.1 Testing the Prototype's Receiver with Static Signals

DC signals were used to measure the static performance of the system. This allowed measuring the amplifying, sampling and conversion noise without the effect of distortion and/or ringing possibly induced by a dynamic signal. The measurements were done with different setups, including one with a standard sensor, one without a cable and one with nothing connected to the board.

In effect, only a zero input signal was used for a simple reason: most of the low frequency noise of the signal chain is removed when subtracting ambient from the signal, which means that a non-zero DC signal would either still result in zero output because of the "ambient" removal or be incomparable because of unremoved low frequency noise.

The measurements were done as a set of series, varying one parameter in each. Figures 24 and 26 show the most important results: The performance proved to be acceptable with low gains but not good enough with higher ones, the target being a standard deviation of 13 LSB or less. Figure 26 proved that shot noise originating from the photodetector is not significant as increasing sampling time and thus effectively decreasing the system's bandwidth has no significant effect on the total noise. As the R_f dependent noise was dominating it was suggested that the differential amplifier selected by the hardware team might not be ideal for this chip.

The theory prompted a test to see what was the actual quality of the input signal. For that, two special cases of measurement setups were built: one with a sensor head soldered right into the connector and encased in tinfoil eliminating all possible interference caused by the sensor cable, and one without anything at all connected to the board. Figure 25 shows the differences of the setups – it can easily be seen that noise in input (which shows as R_f-dependent) is increased when the cable is attached, disturbing the measurement when using higher gains. The increase in noise is due to electrical interference induced in the cable, and it was concluded that the R_f-dependent noise was mostly external rather than caused by the chip itself.

Figure 26 also proves that the chip has some properties ideal for low-power use: the settling times of the receiver chain are low which means that pulse length isn't an important factor in the total performance, enabling very short pulses and thus small duty ratios.

Figure 24 also indicates that using a higher pulse repetition frequency has a positive effect on the performance, as expected, since decimating the signal to the target output frequency allows for filtering and averaging. An important notion

Figure 24: *Receiver noise as a function of gain with several pulse repetition frequencies. The results are analogous to the theoretical model in figure 22, showing a constant and an R_f dependent noise component. Also it can be seen that the performance is better with a higher pulse repetition frequency.*

Figure 25: *The effect of cable and sensor on receiver noise.*

is that the system's settling times are independent of sampling frequency, meaning that the same pulse width can be maintained regardless of PRF, resulting in the fact that lower PRF means a lower duty ratio and therefore lower power consumption – clearly indicating a trade-off between performance and low power usage.

Figure 26: *Receiver noise as a function of pulse width with several pulse repetition frequencies. The results show that above a certain lower limit increasing the width of the sampling window doesn't significantly affect the receiver's performance.*

7.2 Testing the Transmitter Only

The transmitter was tested with a test setup shown in figure 27, the point being to provide the receiver with a zero-mean signal that had all the transmitter's noise. Assuming RMS behavior, it was possible to estimate the noise behavior of the transmitter when outputting a DC signal. Figure 28 shows that the transmitter's signal-to-noise ratio is rather constant and high (115 dB), proving that the receiver is the system's bottleneck. It's to be noted that there's a bit more noise when using a combination of diodes and a resistor as the load – this is natural since with the diodes in place there's a constant additional voltage drop, meaning that the system has to be driven with a larger voltage throughout the current scale.

The transmitter was also tested for its linearity using a standard sensor. It had to be done with a pulsed signal as a DC current of more than 50 mA would probably have burned the sensor during the test. Current linearity is important since with a well-behaving transmitter it's easier to adapt to changing conditions without disturbing the S_pO_2 algorithm. Figure 29 shows the relationship between the LED current setting and the measurement, and it can be seen that it is very linear. Only with added resistance does the curve stray from the optimum, mostly due to limited drive voltage.

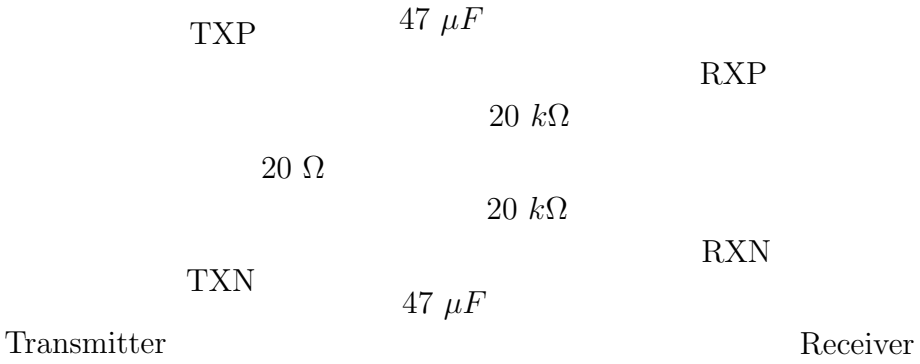

Figure 27: *The test setup of the transmitter using DC current. The circuit eliminates the DC part and passes only the AC signal, i.e. transmitter noise. The 20 Ω resistor can be replaced with a number of diodes and a smaller resistor to simulate the voltage-current response of an actual sensor.*

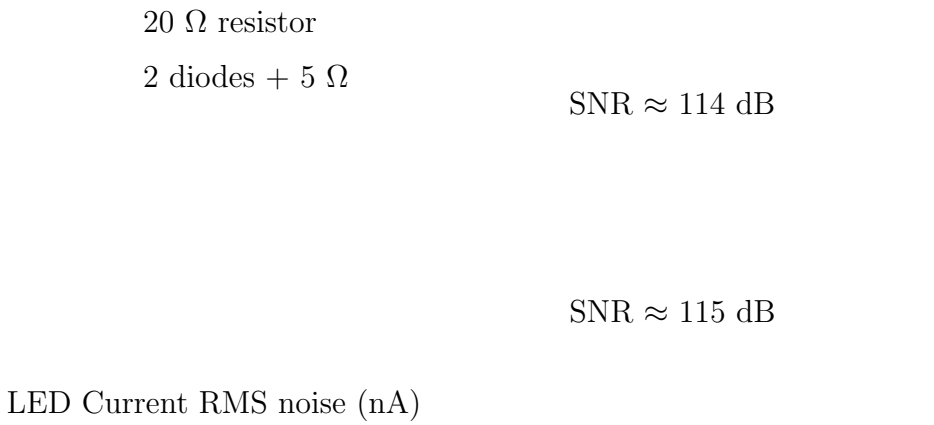

Figure 28: *The calculated transmitter noise as a function of current, measured using the test setup in figure 27.*

7.3 Testing the Prototype with Pulsed Signals

The testing of the system's dynamic properties was begun by measuring system noise with different pulsed LED currents and continued by measuring system noise with a constant pulsed LED current as a function of receiver gain. The tests show that the system's performance drops significantly when a pulsed LED current is introduced in the equation (figure 30), suggesting that there's something wrong with the dynamic properties of either the receiver or the transmitter. To resolve the root cause, the transmitter was measured alone with an external ADC and was found to behave

well throughout the current range, leaving the receiver as the only option. Also the spectral power distribution of the system noise was examined to locate the band of interest.

7.3.1 Crosstalk Between the Transmitter and the Receiver

As the noise of the system increased as a function of transmitter current it was hypothesized that there might be some unwanted crosstalk between the transmitter and the receiver. Their coupling through other paths than through the LED-photodetector interface was tested by blocking the photodetector completely and measuring the signal and system noise with different current settings. With this test it was possible to conclude if the transmitter signal would affect the measurement through some coupling on the board on in the cable. Figure 31 shows that there's no notable effect of this sort.

7.3.2 Ambient Subtraction and Noise Correlation

Crosstalk didn't provide any new insight to the performance problem so the matter was investigated further. From previous measurements it especially stood out that the ambient subtraction didn't seem to perform optimally, leaving low frequency noise in the output signal. The evaluation software was modified to allow examining the individual ambient and channel measurements separately instead of just looking at the final, subtracted signal, and an interesting phenomenon was discovered: the correlation of the noises in the signals decreased as the channel signal level increased,

Figure 29: *The linearity of the transmitter with normal measurement configuration and with added resistance. Nonlinearity with high currents and an added resistance is due to limited drive voltage.*

Figure 30: *System noise as a function of LED current. It can be seen that system performance drops significantly once LED current is introduced, indicating that the dynamic properties of either the receiver or the transmitter are below specification.*

Figure 31: *Signal level and system noise as a function of LED current when the photodetector is blocked. Conclusion: no significant crosstalk between the transmitter and the receiver.*

making system noise reduction by ambient subtraction less efficient.

As the transmitter had already been ruled out as the noise source, it was concluded that the noise properties of some component in the receiver chain depended either on the amplitude of the continuous, pulsed signal or the DC levels of the sampled signals. Figure 32 visualizes the correlation of the noises in the red and the red ambient channels as a function of signal level, showing that even at zero signal the correlation is below 70%. This narrowed the focus to the receiver chain after the amplifier, mainly the sampling and conversion circuits. Figure 33 on the other hand shows the result of low correlation of the channels: as the signal level in the red channel is increased its noise increases as well while the noise of the ambient channel remains relatively constant, and as a result the noise advantage gained from subtracting the two signals becomes smaller and smaller.

From a signal processing perspective, the whole content of the ambient channel is noise that doesn't bear any valuable information but only disturbs the measurement,

Figure 32: *The correlation of the red signal noise and the corresponding ambient signal noise in the target bandwidth as a function of signal level. The graph shows that as signal level grows the correlation decreases, indicating a noise source that only affects one of the signals.*

Figure 33: *The noises of the red and red ambient signals and also the noise of the signal resulting from subtracting the latter from the former. The graph shows that as signal level increases the efficiency of noise reduction by subtraction drops. This is due to decreased correlation between the channels as indicated in figure 32.*

and therefore should be completely removed from the information-carrying signal. On the other hand, the noise in the channels has two components: one that has a common source and therefore correlates, and one that doesn't. In signal subtraction the correlated noise is diminished and the uncorrelated one increased, meaning that the noise minimum is reached by using a scaling factor between zero and one for the ambient that depends on the ratio of correlated and uncorrelated noise. As figure 33 showed that the absolute noise level of the ambient channel is rather constant throughout the signal scale, the conformity of the curves in figure 34 indicates that only the uncorrelated noise increases in the signal channel when signal level is increased. It would suggest that something in or after the sample-and-hold circuits has a signal level dependent noise behavior.

Increasing sampling time was not found to improve the situation after a certain minimum value so the focus was shifted to the ADC and its buffer. As the ADC is a precision part capable of much higher sample rates than with which it is used in the application studied, the quality of the buffer circuitry was questioned. At this point the data gathered was turned over to the hardware team for them to study.

Figure 34: *The noise of the processed signal as a function of ambient scaling. The results show that the ambient channel signal path amplifies the common-mode noise significantly compared to the red channel, the noise in the processed signal having a minimum at a scaling factor around 0.7 even when measuring a zero signal.*

7.4 Conclusion of the First Testing Round

The static tests showed that the new hardware has the potential to meet its specifications and they were also used to find the optimal operating parameters. On the other hand, the dynamic tests showed a significant decrease in performance when using the AFE in a normal pulsed current mode, indicating a flaw in the receiver's sampling and conversion circuitry. The data led to a conclusion that the receiver's signal chain was flawed and didn't handle a pulsed signal well. It was also concluded that said flaw would most probably be found in the buffer feeding the ADC or somewhere nearby.

The conclusion with data to support it was delivered to the hardware team which after considerable time indeed identified a defect in the buffer, proving the hypothesis true. The buffer couldn't properly handle the square-wave resulting from the subsequent conversion of signal and ambient channels; instead it added a considerable amount of noise on top of the wave but not on the bottom, resulting in that the noises in the two channels didn't correlate. Therefore when subtracting ambient the system's low frequency noise didn't cancel itself out as much as planned.

The hardware team implemented a temporary fix to test the impact of the matter. Figure 35 shows that the fix greatly improved system performance when dealing with high signals. There still exists a linear current-noise relationship but its magnitude is significantly lower than before and could diminish even further once the fix is properly implemented.

Figure 35: *System noise as a function of LED current before and after the temporary fix of the ADC's buffer. The results show that the fix improved the system's noise performance.*

7.5 Suitability for Low Power Applications

After having determined that the performance of the AFE looked good enough for performance applications, it was time to decide whether the design concept as a whole suited the needs of the business. The key point in this was that in the optimal case the system would deliver a measurement good enough in all the different use cases (performance, low power, ultra-low power for wireless) with a reasonable price.

7.5.1 Minimum Power Requirements

The absolute minimum power the front-end can be operated with is set by the constant power consumption of the transmitter, the receiver and the microcontroller, totaling in ca. 6 mW. In addition to that, the system also needs power to feed the LEDs – the general rule is that the more power is put into them the better signal-to-noise ratio is achieved, thus making the measurement more accurate. So far the absolute minimum LED power with which a typical finger can be measured is in the range of 1 mW but it only works reliably in the optimal case; typically the LEDs operate with 10-150 mW of power.

7.5.2 Minimum Signal-to-Noise Ratio in Practice

As explained in section 4, the system needs to report the patient's S_pO_2 value with no more than 2 %-points of error. This is interpreted so that taking into account physical variability the standard deviation of the S_pO_2 value must be less than 1 %-point during a period of time, assuming that the mean value is static and reported correctly. In practice this means that the patient's blood perfusion has a lower limit after which the system's signal-to-noise ratio is too low for accurate measuring. Many manufacturers use a Bio-Tek S_pO_2 simulator [43] to validate their low perfusion claims but it was found that the simulator itself produces more noise than the system to be tested as can be seen in figure 36; this prompted new methods for assessing the system's limits.

Having the system's theory in a good shape, the Bio-Tek simulator was used a bit differently: depending on the modulation settings the signal quality varied and subsequently the S_pO_2 algorithm provided readings of different standard deviations. The actual noise level of each of the signals was calculated by fitting an ideal simulator output signal on the data and subtracting it, leaving only noise from the simulator itself and the system. Thus it was possible to draw a relationship between system performance (or signal quality) as seen by the algorithm and S_pO_2 variability which is shown in figure 37.

The data clearly follows a 1/SNR type curve. From the curve it can be concluded that the IR AC signal needs to be 26 times bigger than RMS noise, or in other words the SNR_{AC} has to be at least 26, to achieve an S_pO_2 standard deviation of 1 %-point. This value was fixed to draw a relationship between system noise requirements and IR modulation as per equation (25), shown in figure 38. Overall, for an IR modulation of 0.02% this means that the system's total SNR has to be at least 102 dB. It's more than predicted in figure 16 but it's to be noted that the

Figure 36: *The noises of two measurements with same AFE settings and signal levels, one using the Bio-Tek simulator in DC mode and one using just a light attenuation block in the sensor. It can be seen that the Bio-Tek simulator introduces a lot of noise into the system, rendering direct low perfusion performance tests pointless.*

noise isn't white when using the simulator – due to its properties a lot of the noise is in the fundamental frequency, effectively increasing the value of β in table 1.

$$SNR_{AC} = \frac{I_{AC}}{I_n} = \frac{m_{IR} \cdot I_{DC}}{I_n} \rightarrow I_n = \frac{m_{IR} \cdot I_{DC}}{SNR_{AC}} \tag{25}$$

Figure 37: *The relationship between the effective AC signal-to-noise ratio and S_pO_2 standard deviation. A 1/SNR curve was fitted on the measurement data. The data shows that to achieve S_pO_2 standard deviation of 1 or smaller the AC peak-to-peak signal has to be at least 26 times bigger than RMS noise. For an IR modulation of 0.02% this translates to a SNR requirement of 102 dB.*

Figure 38: *System maximum noise allowed for a reliable measurement as a function of IR modulation as per equation 25. SNR_{AC} is fixed to 26.45.*

8 Discussion

The results obtained from empirical measurements in section 7 are consistent and show that the first prototype of the system doesn't perform optimally and therefore can't be approved. On the other hand, the tests performed using a zero input signal were promising and showed that the system has the potential to be very good. Also the fix implemented by the hardware team shows promising results and it's very probable that the second prototype will fulfill the requirements set for it. The fact that the transmitter exhibits a constant SNR of 115 dB, high compared to the 100 dB of the receiver, leads to the assumption that once the receiver is fixed the total system performance will resemble the first prototype's performance measured with zero current. The following speculations are based on this prerequisite.

8.1 Power vs. Performance Trade-Off

When using a fixed S_pO_2 standard deviation limit the minimum measurable IR modulation is the best indicator of system performance – it sets the actual operating limit of the device. Figure 38 shows the maximum noise level of the system to reliably measure S_pO_2 from a signal with a certain IR modulation, and if it's assumed that the system performance after the ADC buffer fix will be as good as the measurements done with a zero signal, those measurement results can be used to estimate the total system power needed to achieve a certain noise performance. These two data sets combined provide table 2 that links system power for a typical patient and minimum measurable IR modulation. It can be seen that system performance is excellent even when using minimal power, although to achieve the best possible performance a lot of power has to be used. This was to be expected as discussed in section 3. The relationship between power and performance is somewhat a $1/m_{IR}$ type curve, shown in figure 39.

Table 2: *The relationship between system settings, power and low perfusion performance.*

F_s (Hz)	R_f (kΩ)	I_{LED} (mA)	P (mW)	σ (LSB)	Min m_{IR} (%)
625	50	150	125	9.5	0.021
625	100	75	65	9.9	0.022
625	250	35	34	13	0.029
225	250	35	16	16	0.035
225	500	20	12	21	0.046
225	1000	10	9	33	0.073

8.2 Additional Control Parameters

In previous sections it was assumed that there are no obstructions for controlling the system so that the signal mean always stays around the middle of the ADC range. There can be situations, though, where large gains can't be used due to intense ambient light: as large gain also amplifies the ambient level it could be that

Figure 39: *Required system power as a function of IR modulation as listed in table 2.*

the system's dynamic range is too narrow with high gain in some OR applications. Combined with pigmented skin and a thick measurement site it could be that even the selected power mode's maximum current isn't enough to drive the signal to the optimal range. This leads to the fact that measurement SNR drops due to the reduced signal level and has to be taken into account when controlling the system. In effect this is done by measuring the ambient light, setting a maximum gain value based on its level and notifying the host if system performance is limited by the power settings. The host can then decide if it's needed to use more power or not.

8.3 Using the System as a Stand-Alone Product

The MSP430 microcontroller has some computing power reserves that aren't used for measurement control. Therefore it could be possible to construct an extremely small and power-efficient solution that does all signal processing using the MSP430. The downside is that since the microcontroller doesn't support hardware division or floating point calculation the algorithm would have to be a heavily stripped-down version with reduced performance. Again, the trade-off between power, size and performance is clear and it's up to the application specifications if the performance provided is enough or not. For example, some home monitoring solutions could do with a very simple algorithm as the patient is not expected to be in a low perfusion state – such solution would have a greatly extended battery life and improved portability compared to more traditional monitors.

9 Conclusions

The work done in this thesis was a part of a project which develops a new generation of pulse oximetry measurement hardware. The development model of the embedded software used with the hardware was fine-tuned to serve both the evaluation process and product development, and indeed most of the software developed for the purpose of performance evaluation will also be used in the final product. The performance analysis results themselves were essential in the hardware evaluation process – in fact, they clearly pointed out a flaw in the design that otherwise probably would have gone unnoticed. The analysis had to be done using a black box approach due to the hardware being tightly packed and shielded, rendering measurements of the individual subsystems impossible to do; that is why the output of the system's ADC was the only data source used.

9.1 Software

A completely new piece of embedded software was written for the new measurement circuit's microcontroller using Embedded C++ and object-oriented design. The software has total control of the hardware, taking care of the timing and signal levels of the pulse oximetry measurement and handling communication between the measurement circuit and the host. Hardware timers, DMA and interrupts were used. The development of the software and especially the priority order of certain components was highly guided by the evaluation process, yet everything was done keeping in mind that the result would be a usable and maintainable final product. The goal was reached very well.

In addition to the embedded software, also a host program with a graphical user interface was written using Matlab. It served as a signal acquisition and data analysis tool during the verification process, providing a two-way interface to the measurement circuit. A lot of the tool's code can most probably be re-used in further evaluations as only the hardware setting editor is system-dependent.

9.2 Performance Analysis

Noise requirements for the hardware were calculated based on the signal processing algorithm used and the performance specifications of the S_pO_2 measurement. The results were that a signal-to-noise ratio of ca. 98 dB would be required to reliably measure S_pO_2 from a low perfusion pleth signal with IR modulation of 0.02%. This was also tested empirically and it was concluded that a signal-to-noise ratio of approximately 100 dB was needed when using a simulator to generate the pleth waveform; the setting also represents a bad-case scenario as the simulator's spectral noise distribution has significant spikes at the fundamental cardiac frequency and its harmonics.

The performance of the hardware was assessed by systematically measuring the amount of noise present in the output signal with different system settings. By fitting the results to the model of the system it was possible to pinpoint the major

sources of noise, i.e. the parts of the system that weren't performing optimally. The measurements were made as sets, modifying only one operating parameter in each. The most important parameters were receiver gain, sampling time, LED current and sensor type.

The performance tests showed that the receiver performed well with a DC signal. Once a pulsed signal which is used in normal operation was introduced the performance dropped significantly. The tests ruled out the transmitter as the noise source, indicating that a component in the receiver chain was flawed. In addition to measuring the noise present in the output signal, the correlation of different channels was examined as well to prove that the observed added noise component in the signal channel didn't correlate with its corresponding ambient channel and therefore was most likely thermal noise affecting only one of the signals or noise the magnitude of which depended on the signal level. Further on, the tests allowed to isolate the problem in the sampling and conversion units. Finally the bug was found in the buffer feeding the ADC and a fix was made by the hardware team, increasing system performance significantly.

In the end it was determined that the new measurement circuit will fulfill the design specifications set for it after the bugs found are fixed. The circuit will be used in a range of GE's upcoming products.

References

[1] Gerard J. Tortora and Sandra Reynolds Grabowski. *Principles of Anatomy and Physiology*. John Wiley & Sons, Inc., New York, 9th edition, 2000.

[2] The cardiovascular system. `http://www.urgomedical.com/var/ezflow_site/storage/images/media/images/venous-system-02/2059-1-eng-GB/venous-system-02.jpg`, referred July 11th, 2011.

[3] Hemoglobin. `http://mycozynook.com/22_11HemoglobinO2-L.jpg`, referred July 11th, 2011.

[4] Red blood cells. `http://images.medicinenet.com/images/illustrations/blood_cells.jpg`, referred July 11th, 2011.

[5] John G. Webster. *Design of Pulse Oximeters*. Institute of Physics Publishing, Bristol and Philadelphia, 1997.

[6] The respiratory system. `http://commons.wikimedia.org/wiki/File:Illu_bronchi_lungs.jpg`, referred July 11th, 2011.

[7] D. Thomas. The physiology of oxygen delivery. *Vox Sanguinis*, 87:70–73, 2004.

[8] Hemoglobin saturation curve. `http://www.molecularstation.com/molecular-biology-images/data//505/Hb-saturation-curve.png`, referred July 11th, 2011.

[9] Ellison C. Pierce. Pro: Is pulse oximetry still worthwhile? *Journal of Clinical Monitoring and Computing*, 14:367–368, 1998. 10.1023/A:1009939627223.

[10] Richard W. Morris, Alan Buschman, Diane L. Warren, James H. Philip, and Daniel B. Raemer. The prevalence of hypoxemia detected by pulse oximetry during recovery from anesthesia. *Journal of Clinical Monitoring and Computing*, 4:16–20, 1987. 10.1007/BF01618102.

[11] Watson A. Bowes, Barry C. Corke, and Jaroslav Hulka. Pulse oximetry: A review of the theory, accuracy, and clinical applications. *Obstetrics and Gynecology*, 74(3, Part 2):541–546, 1989.

[12] History of oximetry. `http://www.oximetry.org/pulseox/history.htm`, referred July 11th, 2011.

[13] Takuo Aoyagi, Masayoshi Fuse, Naoki Kobayashi, Kazuko Machida, and Katsuyuki Miyasaka. Multiwavelength pulse oximetry: theory for the future. *Anesthesia and analgesia*, 105(6 Suppl):S53–8, tables of contents, December 2007.

[14] M. J. Tobin, editor. *Principles and Practice of Intensive Care Monitoring*. McGraw-Hill, Inc., 1 edition, 1998.

[15] John Allen. Photoplethysmography and its application in clinical physiological measurement. *Physiological Measurement*, 28(3), 2007.

[16] Plethysmographic and electrocardiographic signals. `http://science.kingston.ac.uk/bpsrg/images/ECG.jpg`, referred July 11th, 2011.

[17] Y Mendelson. Pulse oximetry: theory and applications for noninvasive monitoring. *Clinical Chemistry*, 38(9):1601–7, 1992.

[18] ISO 80601-2-61. Medical electrical equipment -Particular requirements for basic safety and essential performance of pulse oximeter equipment. *INTERNATIONAL STANDARD*, 2-61:92, 2011.

[19] Pleth variability index (pvi). Masimo Whitepaper, `http://masimo.com/pdf/whitepaper/LAB4583A.pdf`, referred February 13th, 2012.

[20] J Allen and A Murray. Development of a neural network screening aid for diagnosing lower limb peripheral vascular disease from photoelectric plethysmography pulse waveforms. *Physiological Measurement*, 14(1):13, 1993.

[21] A. C. RALSTON, R. K. WEBB, and W. B. RUNCIMAN. Potential errors in pulse oximetry iii: Effects of interference, dyes, dyshaemoglobins and other pigments*. *Anaesthesia*, 46(4):291–295, 1991.

[22] J Lee. Design of filter to reject motion artifact of pulse oximetry. *Computer Standards & Interfaces*, 26(3):241–249, May 2004.

[23] Steven J. Barker and Kevin K. A Tremper. The effect of carbon monoxide inhalation on pulse oximetry and transcutaneous po2. *Anesthesiology*, 66(5):677–679, 1987.

[24] S.J. Barker, K.K. Tremper, and J. Hyatt. Effects of methemoglobinemia on pulse oximetry and mixed venous oximetry. *Anesthesiology*, 70(1):112–117, 1989.

[25] A. Sidi, DA. Paulus, W. Rush, N. Gravenstein, and RF. Davis. Methylene blue and indocyanine green artifactually lower pulse oximetry readings of oxygen saturation. studies in dogs. *Clinical Monitoring*, 3(4):249–256, 1987.

[26] MS. Scheller, RJ. Unger, and MJ. Kelner. Effects of intravenously administered dyes on pulse oximetry readings. *Anesthesiology*, 65(1):550–552, 1986.

[27] N S Trivedi, a F Ghouri, N K Shah, E Lai, and S J Barker. Effects of motion, ambient light, and hypoperfusion on pulse oximeter function. *Journal of clinical anesthesia*, 9(3):179–83, May 1997.

[28] Pulse oximeter block diagram. `http://focus.ti.com/docs/solution/folders/print/330.html`, referred July 13th, 2011.

[29] S A Maas. *Noise in linear and nonlinear circuits*. Artech House microwave library. Artech House, 2005.

[30] K N Glaros and E M Drakakis. Trade-offs for low power integrated pulse oximeters. In *Biomedical Circuits and Systems Conference, 2009. BioCAS 2009. IEEE*, pages 245–248, 2009.

[31] Tram - high acuity patient monitoring. `http://www.gehealthcare.com/euen/patient_monitoring/docs/Tram_spec_e.pdf`, referred Dec 29th, 2011.

[32] John E. Scharf, Stephan Athan, and David Cain. Pulse Oximetry Through Spectral Analysis. In *Twelfth Southern Biomedical Engineering Conference*, pages 227–229, 1993.

[33] Photodiode characteristics. OSI Optoelectronics Application Note, `http://www.osioptoelectronics.no/application-notes/AN-Photodiode-Parameters-Characteristics.pdf`.

[34] National semiconductor lmp7731 precision operational amplifier. `http://www.national.com/pf/LM/LMP7731.html`, referred February 9th, 2012.

[35] M. Schwartz. *Information transmission, modulation, and noise*. McGraw-Hill series in electrical engineering. McGraw-Hill, 1990.

[36] Yingkun Gai, Randall Geiger, and Degang Chen. Noise Analysis in Hold Phase for Switched-Capacitor Circuits. In *51st Midwest Symposium on Circuits and Systems*, pages 45–48, 2008.

[37] Pervez M Aziz, Henrik V Sorensen, and J van der Spiegel. An Overview of Sigma-Delta Converters. *IEEE Signal Processing Magazine*, 13(January):61–84, 1996.

[38] Msp430f5529 microcontroller product information. `http://focus.ti.com/docs/prod/folders/print/msp430f5529.html`, referred August 15th, 2011.

[39] ATMEL. AT91 ARM Thumb-based Microcontrollers, AT91SAM9261 Preliminary. *Data Sheet*, page 749, 2009.

[40] D.G. Kleinbaum, L.L. Kupper, and K.E. Muller. *Applied regression analysis and other multivariable methods*. Duxbury applied series. Brooks/Cole, 2007.

[41] K. Schwaber. *Agile Project Management with Scrum*. O'Reilly Media, Inc., 2009.

[42] Iar embedded workbench for msp430. `http://www.iar.com/en/Products/IAR-Embedded-Workbench/TI-MSP430/`, referred Dec 29th, 2011.

[43] Bio-tek instruments fda 510(k) k971273. `http://www.accessdata.fda.gov/cdrh_docs/pdf/K971273.pdf`, referred February 10th, 2012.